High-Order Disclinations in the Polarization of Light

Enrique J. Galvez,[1] and Behzad Khajavi,[1,2]
[1]Department of Physics and Astronomy, Colgate University, Hamilton, NY 13346, U.S.A.
[2]Department of Physics and Astronomy, Florida Atlantic University, Boca Raton, FL 33431, U.S.A.

ABSTRACT

We present modelings of high-order line singularities encoded in space-variant polarization of light. This involves calculating the line patterns produced by the superposition of light beams in orthogonal states of circular polarization, with each beam carrying an optical vortex, and where one of them is asymmetric. This setting allowed us to study the case of monstars of high order. We find that monstars can have positive or negative singularity indices, modifying the previous understanding of the pattern, which was based on the case of lowest-order C-points. Monstars then remain characterized only by their own unique feature: sectors with patterns of mostly curved lines that radiate from the center. Given this definition, we propose that the case where the index is +1 be classified as a monstar. We also found that the asymmetric modes contain kinks that appear in the C-lines of a distinct but related pattern that contains line orientation discontinuities.

Keywords: Polarization singularities, C-points, Monstars, Disclinations

1. INTRODUCTION

Polarization singularities have become increasingly important in light of newly developed methods to produce designer beams carrying space-variant polarization. Such beams can be produced either by superposition of optical beams;[1–7] or by passage through q-plates,[8,9] optical elements with stress birefringence,[10] optical fibers,[11,12] or subwavelength gratings.[13] These methods allow a greater exploration of disclinations, which are ubiquitous in nature, as well as providing a setting for applications. In the case of light, orientation polarization singularities come in the form of C-points,[14] and which are classified as lemons, stars and monstars.[15–17] Not until recently have monstars, a purely asymmetric C-point, have been realized in the laboratory.[4,5] Most of these demonstrations have involved first-order singularities. Some higher-order singularities have been investigated in the context of vector beams,[8] but none have been investigated in Poincaré beams.

In this study we present a study of the generation of Poincaré beams with high-order C-points, both symmetric and asymmetric. We do this by exploring the superpositions of two Laguerre-Gauss modes in orthogonal states of circular polarization. By varying the asymmetry of one of the beams we are able to generate new asymmetric patterns not seen before.

2. BASIC RELATIONS

This work follows previous research on polarization singularities, where we studied lowest-order C-points[3,5] and composite C-points.[6] Here we focus on the case of high-order C-points, also known as hyper-C-points.[18] We also investigate the full spectrum of asymmetric C-points and the range of conditions that produce monstars. We also want to point out that C-points are a manifestation of a more general phenomenon of disclinations and orientation singularities. Our analysis will use disclination patterns to get a clearer view of the line structure that underlies the polarization patterns.

The beams of light are in a general non-separable superposition of polarization and spatial mode given by

$$U = \left(\cos\beta\ LG_0^{\ell_1} + \sin\beta\ LG_0^{-\ell_1}\ e^{\mathrm{i}\gamma}\right)\ \hat{e}_R + LG_0^{\ell_2}\ e^{\mathrm{i}\delta}\ \hat{e}_L, \tag{1}$$

Further author information: (Send correspondence to E.J.G.)
E.J.G.: E-mail: egalvez@colgate.edu, Telephone: 1 315 228 7205
Proceedings of SPIE **9764**, 97640R (2016).

where β, γ and δ are phases that we can vary; $\hat{e}_R$ and $\hat{e}_L$ represent the polarization states of right and left circular polarization, respectively; and LG_0^ℓ is a Laguerre-Gauss spatial mode with zero radial index (entailing singly ringed "doughnut" transverse amplitudes) and topological charge ℓ. The spatial mode is given by[3]

$$LG_0^\ell = A_\ell r^{|\ell|} e^{i\ell\phi} GW, \tag{2}$$

where r and ϕ are the transverse polar coordinates; A_ℓ is the amplitude of the mode, given by

$$A_\ell = \left(\frac{2^{|\ell|+1}}{\pi|\ell|!}\right)^{\frac{1}{2}} \left(\frac{1}{w}\right)^{|\ell|+1}, \tag{3}$$

with w being the half-width of the mode; G is the Gaussian function

$$G = e^{-r^2/w^2}; \tag{4}$$

and W is the transverse phase propagator, given by

$$W = e^{\mathrm{i}[kr^2/(2R)+\varphi]}, \tag{5}$$

where k is the wave vector, R the radius of curvature of the wavefront, and φ the Gouy phase.

3. C-POINTS

The superposition of Eq. 1 produces in general a Poincaré beam. That is, a beam with space variant polarization that conveys a mapping of the Poincaré sphere onto the transverse mode of the light.[3] As is well known, the orientation of the semi-major axis of the polarization is half of the relative phase between the two circular polarization components in Eq. 1. When either $\beta = 0$ or $\beta = 90°$ the orientation is

$$\theta = \frac{1}{2}(\Delta\ell\phi - 2n\pi), \tag{6}$$

where n is an integer, and where $\Delta\ell = \pm\ell_1 - \ell_2$ (the sign of ℓ_1 is positive for $\beta = 0$ and negative for $\beta = 90°$). Because the the orientation varies with the transverse angular coordinate, the center of the beam is a polarization singularity, or C-point.[17] Note also that the orientation is independent of the radial coordinate r.

The C-point is categorized by its index, which is the number of times that the orientation rotates per turn around the C-point

$$I_C = \frac{\Delta\theta}{2\pi}, \tag{7}$$

or

$$I_C = \frac{\Delta\ell}{2}. \tag{8}$$

Let us consider the simplest particular case of Eq. 1 involving $\ell_1 = 1$ and $\ell_2 = 0$. When $\beta = 0$ or $\beta = 90°$, the mode is produced by a symmetric optical vortex in a state of right circular polarization superimposed with a mode with a planar wavefront and left circular polarization. This gives rise to a C-point pattern that is symmetric, where the rate of change of the orientation with the angular coordinate is linear, as seen in Eq. 6. The case $\ell_1 = 1$ and $\ell_2 = 0$ produces the smallest absolute value of I_C: 1/2. This is when the ellipse rotates by half a turn when following a closed path around the C-point. When $I_C = +1/2$, the symmetric pattern is called a lemon. This is illustrated by arrows in corresponding left-most pattern shown in Fig. 1. When $I_C = -1/2$, the symmetric pattern is called a star. Lemons and stars can be asymmetric. In asymmetric cases the line orientation changes nonlinearly with ϕ. Monstar is a third type of line singularity with similarities to both lemons and stars, but also with unique features of its own.

The number of radial lines represent directions where the semi-major axes of the polarization ellipses are radial. The lowest-order lemon, with $I_C = +1/2$, has one radial line; and the lowest-order star, with $I_C = -1/2$, has 3 radial lines. For a range of values of β the pattern has $I_C = +1/2$ but 3 radial lines. This pattern is the

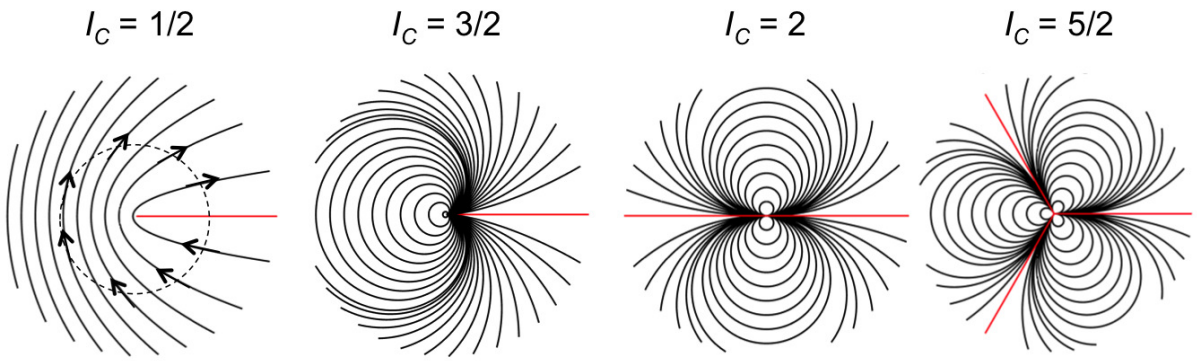

Figure 1. Line singularity patterns for the lowest-order hyperlemons created by superpositions of topological charges (ℓ_1, ℓ_2) and $\beta = 0$ in Eq. 1, producing a pattern with index I_C. The cases shown are: $I_C = 1/2$ with $(1, 0)$; $I_C = 3/2$ with $(2, -1)$; $I_C = 2$ with $(3, -1)$; and $I_C = 5/2$ with $(1, -4)$. Red solid lines denote radial lines. The case for $I_C = 1/2$ has arrows added to it to illustrate the rotation of the polarization around the C-point.

monstar.[15] Up to now, this notion has become the default definition of monstars: same index as the lemon and same number of radial lines as the star. Monstars also have a separate distinctive feature that seem to be their only defining property: sectored radiations.

We can define more accurately the number of radial lines for the symmetric cases (i.e., $\beta = 0, 90°$). The values of ϕ for which there is a radial line is obtained by equating:

$$\theta = \phi. \tag{9}$$

The solutions are

$$\phi_r = \frac{2n\pi - \delta}{2 - \Delta\ell} \tag{10}$$

Except for the case with $I_C = 1$, the number of radial lines is given by

$$N = |2(I_C - 1)| = |2 - \Delta\ell| \tag{11}$$

In particular, we will often use the values of I_C and N_β for the symmetric cases at $\beta = 0$ and $\beta = 90°$:

$$I_{C,0} = \frac{\ell_1 - \ell_2}{2} \tag{12}$$

$$N_0 = 2 - \ell_1 + \ell_2 \tag{13}$$

$$I_{C,90} = \frac{-\ell_1 - \ell_2}{2} \tag{14}$$

$$N_{90} = 2 + \ell_1 + \ell_2 \tag{15}$$

Lemons with index higher than 1/2 index are known hyperlemons.[18] In Fig. 1 we show the line patterns of hyperlemons of increasing index. For lemons with $I_C > 1/2$, the main characteristic is the pattern of closed curves that begin and end at the center of the pattern, also referred to as flower petals.[18] They are numerically the same as the number of radial lines (red in the figure). Thus hyperlemons can have more than one radial line. Although we have not confirmed this analytically, the patterns for $I_C = +3/2$, $I_C = +2$ and $I_C = +5/2$ appear to have the form of cardioids, circles and rose petals, respectively. The line structure for a given value of I_C is the same for combinations of vortices that have the same value of $\Delta\ell$. For example, $\Delta\ell = 3$ gives rise to the pattern for $I_C = +3/2$, which can be implemented for $\beta = 0$ by values of (ℓ_1, ℓ_2) given by $(2, -1)$, $(3, 0)$ and $(4, 1)$. While the orientation patterns for these cases are the same, the ellipticity patterns are not, because the ellipticity is given by[3]

$$\epsilon = \pm\frac{b}{a} = \tan(\pi/4 - \chi), \tag{16}$$

where a and b are the semi-minor and semi-major axes of the ellipse, and

$$\chi = \tan^{-1} \frac{A_{0,\ell_2} r^{|\ell_2|}}{A_{0,\ell_1} r^{|\ell_1|}}. \tag{17}$$

Thus, the ellipticity of the patterns depends on the particular pair of modes used.

Similarly to lemons, the index for hyperstars is $I_C < -1/2$. Figure 2 shows examples of hyperstars with the lowest values of $|I_C|$. Stars are characterized by the number of points, which is the same as the number of radial lines. They have been referred to before as "spider webs."[18]

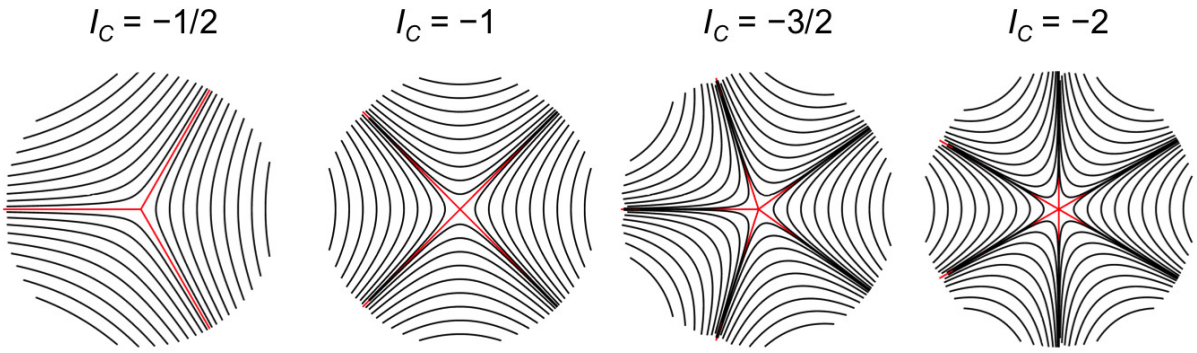

Figure 2. Line singularity patterns for the lowest-order hyperstar, created by superpositions of topological charges (ℓ_1, ℓ_2) and $\beta = 90°$ in Eq. 1, producing a pattern with index I_C. The cases shown are: $I_C = -1/2$ with $(1, 0)$; $I_C = -1$ with $(3, -1)$; $I_C = -3/2$ with $(2, 1)$; and $I_C = -2$ with $(4, 0)$. Red solid lines denote radial lines.

4. TRANSITIONAL PATTERNS AND MONSTARS

We have seen for the lowest-order case, monstars are transitional patterns that appear between lemons and stars. These are situations where the number of radial lines changes from that of the lemon to that of the star but retaining the same index of the lemon. This is not the case for high-orders, because we can have transitional patterns between two distinct-index lemons as well as between two distinct-index stars. The question driving our work was: Could there exist monstars in these cases? Table 2 shows the possible cases involved in a transition from one C-point to the another. It shows that by suitable choice of ℓ_1 and ℓ_2 we can investigate all the possibilities.

Table 1. Types of transitions via the variation of β in Eq. 1. It uses the definitions of the singularity indices of Eqs. 12 and 14.

Condition	$\beta = 0$		$\beta = \pi/2$	
	$I_{C,0}$	Pattern	$I_{C,90}$	Pattern
$\lvert\ell_1\rvert > \lvert\ell_2\rvert$	> 0	Lemon or Monstar ($I_C = +1$)	< 0	Star
$\lvert\ell_1\rvert < \lvert\ell_2\rvert$, $\ell_2 > 0$	< 0	Star	< 0	Star
$\lvert\ell_1\rvert < \lvert\ell_2\rvert$, $\ell_2 < 0$	> 0	Lemon	> 0	Lemon

For the first case of Table 2, at $\beta = 0$ and $\Delta\ell \neq 2$ ($I_C \neq 1$), the pattern will be one of a lemon or hyper-lemon. As we increase β from zero, the superposition of modes with ℓ_1 and $-\ell_1$ produces an asymmetric lemon C-point of index $I_{C,0}$ with N_0 radial lines when $\beta < \pi/4$; and an asymmetric star of index $I_{C,90}$ with N_{90} radial lines when $\beta > \pi/4$. This asymmetric C-point often but not always gives rise to a monstar transitional pattern. The transition from lemon to monstar occurs for a range of values of β between $\beta = \pi/4$ and a value of β that

depends on γ, which we label β_γ. For the case $(\ell_1, \ell_2) = (1, 0)$ the lowest value of β_γ occurs at $\gamma = \pi$, and the highest value converges to $\pi/4$ as $\gamma \to 0, 2\pi$. At $\gamma = 0$ there are no monstars, and the lemon transforms directly into a star through the intermediate C-line transitional pattern at $\beta = 45°$ (more on this below). In our previous work we calculated $\beta_\gamma = 1/\tan^{-1}(1/3)$ for $\gamma = \pi$,[5] obtained by finding the solutions to Eq. 9 in the problem, which gives rise to a cubic equation in $\sin\phi$.[19]

The more general case of Eq. 9 leads, after some algebra, to the equation:

$$\cos\beta \sin\Psi + \sin\beta \sin\Phi = 0, \tag{18}$$

where

$$\Psi = (\ell_1 - \ell_2 - 2)\phi - \delta + 2n\pi \tag{19}$$

$$\Phi = (-\ell_1 - \ell_2 - 2)\phi + \gamma - \delta + 2n\pi \tag{20}$$

with n integer. Many cases can easily be solved algebraically for simple values of γ. Equation 18 leads to a polynomial equation in powers of $\sin\phi$, of order $N = \max(N_0, N_{90})$. Radicals in the solution give minimum or maximum allowed values of $\beta = \beta_\gamma$ that mark the division between number of radial lines N_0 and N_{90}. This division is the boundary between lemon or star, and monstar. We found that monstars also appear when the extreme symmetric cases are both lemon patterns or both star patterns with distinct number of radial lines. The more general cases can be solved numerically. Table 2 shows the values to β_γ for the lemon-monstar boundaries.

Table 2. Examples of C-point transitions. Specific cases are labeled by the values of ℓ_1 and ℓ_2 in Eq. 1, the parameters of the patterns

Case	(ℓ_1, ℓ_2)	$I_{C,0}$	$I_{C,90}$	N_0	$N_{m,0}$	$N_{m,180}$	N_{90}	β_0	β_{180}
Lemon-Star	$(1, 0)$	$+1/2$	$-1/2$	1	–	3	3	–	18.43°
Lemon-Star	$(2, 1)$	$+1/2$	$-3/2$	1	5	3	5	38.66°	11.31°
Lemon-Star	$(2, -1)$	$+3/2$	$-1/2$	1	3	–	3	18.43°	–
Lemon-Star	$(3, 0)$	$+3/2$	$-3/2$	1	3	5	5	11.31°	38.66°
Lemon-Star	$(3, -1)$	$+2$	-1	2	4	–	4	26.57°	–
Star-Star	$(1, 2)$	$-1/2$	$-3/2$	3	–	3	5	–	31.0°
Star-Star	$(2, 3)$	$-1/2$	$-5/2$	3	7	5	7	41.4°	23.3°
Star-Star	$(1, 3)$	-1	-2	4	–	–	6	–	–
Star-Star	$(1, 4)$	$-3/2$	$-5/2$	5	–	7	7	–	35.6°
Lemon-Lemon	$(1, -2)$	$+3/2$	$+1/2$	1	–	–	1	–	–
Lemon-Lemon	$(2, -3)$	$+5/2$	$+1/2$	3	3	–	1	71.57°	–
Lemon-Lemon	$(1, -4)$	$+5/2$	$+3/2$	3	–	3	1	–	71.57°
Lemon-Lemon	$(3, -4)$	$+7/2$	$+1/2$	5	3	–	1	78.69°	–
Monstar-Star	$(2, 0)$	$+1$	-1	∞	4	4	4	0	0
Monstar-Star	$(3, 1)$	$+1$	-2	∞	6	6	6	0	0

The top third of Table 2 shows the lemon-star cases, with the first row showing the previously studied case.[5, 19] The table lists the values of ℓ_1 and ℓ_2, and the indices of the patterns for $\beta = 0$ and $\beta = 90°$, $I_{C,0}$ and $I_{C,90}$, respectively. These indices also cover the asymmetric regimes for $\beta < 45°$ and $\beta > 45°$, respectively. The remaining columns report on the results of our calculations for monstar patterns, by listing the number of radial lines that the monstar patterns have as well as the threshold values β_γ. Earlier we mentioned that β_γ can have a maximum or a minimum value when γ is either 0 or 180°, respectively. When there are monstars for at least one value of γ, implies these may also exist for other values of γ. When there are no monstars for any value of β for $\gamma = 0, 180°$, we denote it with a dash. As can be seen, every case in this group of transformations has a monstar range.

Frames (a) and (b) of Fig. 3 show monstars for cases $(2, 1)$ and $(3, 0)$, with indices $+1/2$ and $+3/2$, respectively. The case (b) for $(3, 0)$ is quite interesting. For $\beta = 0$ there is one radial line; for $\beta = 90°$ there are 5 radial

lines. There are monstars for both extreme values of γ. However, for $\gamma = 0$ monstars have 3 radial lines and for $\gamma = 180°$ they have 5 radial lines. Thus, the monstar morphs from 3 to 5 radial lines at an intermediate value of γ.

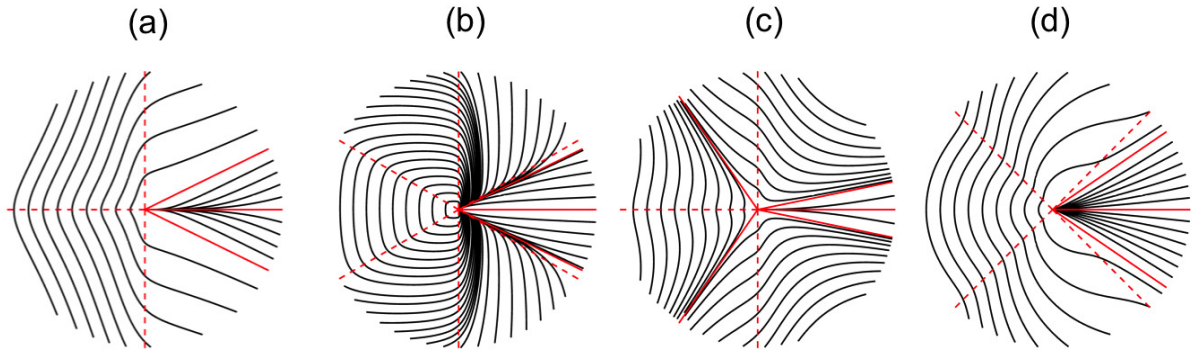

Figure 3. Four examples of monstars: (a) $(\ell_1, \ell_2) = (2, 1)$ for $\beta = 30°$ and $\gamma = 180°$, yielding $I_C = +1/2$; (b) $(\ell_1, \ell_2) = (3, 0)$ for $\beta = 30°$ and $\gamma = 0$, yielding $I_C = +3/2$; (c) $(\ell_1, \ell_2) = (2, 3)$ for $\beta = 30°$ and $\gamma = 180°$, yielding $I_C = -1/2$; and (d) $(\ell_1, \ell_2) = (2, -3)$ for $\beta = 60°$ and $\gamma = 0$, yielding $I_C = +1/2$. Solid red lines are radial lines, and dashed red lines correspond to the C-lines of the corresponding cases with $\beta = 45°$.

The second series of entries in Table 2 are the cases where there are stars at both $\beta = 0$ and $\beta = 90°$. Three of four cases contain monstars. That is, monstars with a negative index. This is quite a surprising result because in the first-order cases the monstar index is positive, and was thought to be a defining property of monstars. Frame (c) of Fig. 3 shows case $(2, 3)$ for $\beta = 30°$ and $\gamma = 180°$. This is a monstar of index $-1/2$. It has 5 radial lines (solid red). Two of those radial lines enclose sectors where lines appear to be radiating from the center. Those sectors do not have the star-like features (hyperbolic-like lines) that avoid the center. This transformation is shown in Fig. 4. It is a case that starts with a $-1/2$ star in frame (a). At $\beta = 23.3°$ two radiating-line sectors grow from one of the radial lines, producing a monstar pattern with a total of 5 radial lines, which grow to the pattern of Fig. 3 (c) at $\beta = 30°$, and reaching the pattern of Fig. 4 (b) at $\beta = 44°$. As β crosses over to $\beta = 46°$ in frame (c), the radiating sectors merge to become one of the hyperbolic sectors of the 7-point star, and with 3 radial lines spontaneously appearing at cusps in the lines when $\beta \to 45°$. As $\beta \to 90°$ the pattern becomes a symmetric 7-point star.

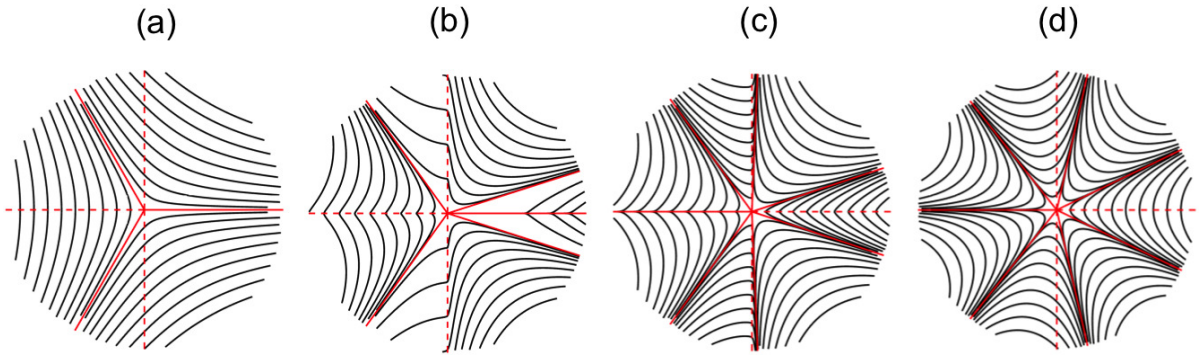

Figure 4. Transformation of a $-1/2$ star to a $-5/2$ star through a monstar. All frames correspond to the case $(2, 3)$ with $\gamma = 180°$. They divide by value of β: 0 for (a), 44° for (b), 46° for (c), and 90° for (d). Red solid lines are radial lines and red dashed lines are C-lines for the $\beta = 45°$ case.

The third set of transformations in the series of entries for Table 2 involve cases where there are lemons at both $\beta = 0$ and $\beta = 90°$. By now, from Eq. 11 and Fig. 1, it must be clear that lemons can have more than one radial line. We find mostars within the regions where lemons have the lower index. This makes sense because when monstars arise they add new sectors, normally in pairs, as far as we can tell, and this addition requires two more radial lines. Eventually some these radial lines morph into the radial lines of the other star pattern. Figure 3 (d) shows the monstar for the case $(2, -3)$ at settings $\beta = 60°$ and $\gamma = 0$. All of the monstars that appear in this set of conditions (third group of Table 2) have lemon-type sectors plus sectors with radiating lines. Thus, in all, the commonality among all the monstar patterns is the sectors with radiating lines.

It might be intriguing that $I_C = 1$ is missing from Fig. 1. That is because we now classify it as a monstar. As shown in the fourth group of Table 2, it appears when $\Delta\ell = 2$ with $\beta = 0$. In this case there is a solution for radial lines only for $\delta = 2n\pi$, a case where there are radial orientations at all the angles, as shown in Fig. 5(a). This is also known as the radial mode, popularized by the case $\ell_1 = -\ell_2 = 1$, and known as the radial vector mode. However, other versions of the radial mode for the case $(2, 0)$ have been shown before.[8] For $|\ell_1| \neq 1$ the semi major axes are radial, but the states are elliptical, with ellipticity depending on the radial coordinate. When $\delta \neq 0$ there are no radial solutions. The case $\delta = \pi$ is also known as the tangential mode because all the semi-major axes are tangential to circles centered at the C-point. When $\delta \neq 0, \pi$ the mode is a swirl,[6] with lines that radiate from the center but that curve around in spiral-like fashion, as shown in Fig. 5(b). The number of turns about the center increases with δ, reaching an infinite number of turns as $\delta \to 180°$. Moreover, when $\delta = 0$ but $\beta \neq 0$, lines radiate from the center as we have seen with other monstars: curved trajectories but with a finite number of them being straight and radial. This is shown in Fig. 5 (c) for $(2, 0)$ with $\beta = 30°$ and $\gamma = 180°$, and (d) for $(3, 1)$ with $\beta = 30°$ and $\gamma = 0°$. The red dashed lines that define the C-lines at $\beta = 45°$ locate one set of radial lines. The directions half-way between these radial lines are also radial. These radial lines may not be structurally robust, because they disappear when we let $\delta \neq 0$. Given the similarities with monstars, we are led to conclude that the $I_C = 1$ case is a form of monstar.

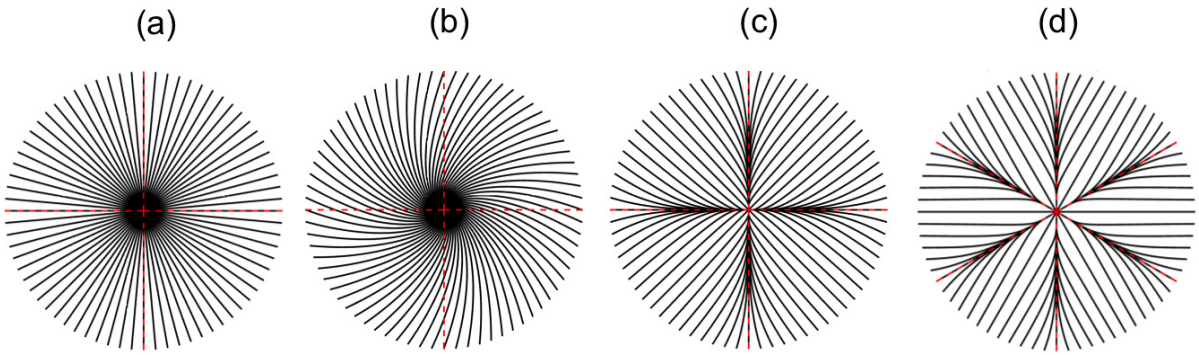

Figure 5. Patterns corresponding to the $I_C = +1$ for the following conditions: (a) $(\ell_1, \ell_2) = (2, 0)$ with $\beta = 0$, $\gamma = 180°$ and $\delta = 0$; (b) $(2, 0)$ with $\beta = 0$, $\gamma = 180°$ and $\delta = 40°$; (c) $(2, 0)$ with $\beta = 30°$, $\gamma = 180°$ and $\delta = 0$; and (d) $(3, 1)$ with $\beta = 30°$, $\gamma = 0$ and $\delta = 0$;

5. C-LINES AND THEIR SCARS

When $\beta = 45°$ a very interesting pattern appears. It does not contain any of the C-points investigated so far. The patterns contain C-lines, which are lines of circular polarization that divide regions that have lines of orientation vary continuously with ϕ. At the C-lines, the orientation of the lines changes discontinuously. The pattern is divided into $2\ell_1$ sectors separated by C-lines. The angles at which the C-lines occur are given by

$$\phi_n = \frac{(2n-1)\pi + \gamma}{2\ell_1}. \tag{21}$$

We can understand this in simple terms by realizing that at the C-lines the amplitude of the right-circular polarization (Eq. 1) is zero. At the C-line, the spatial mode with right-circular polarization undergoes an abrupt phase shift of π. Figure 6 shows an example for the case $(2, -1)$. The intensity pattern in Fig. 6(b) shows the features of the mode in the right-circular state. The mode is a superposition of LG_0^{+2} and LG_0^{-2} with equal magnitudes (i.e., because $\beta = 45°$). The nodes of that mode are the dashed lines in Fig. 6(a). At those points, the polarization is left-circular, provided by the LG_0^{-1} mode.

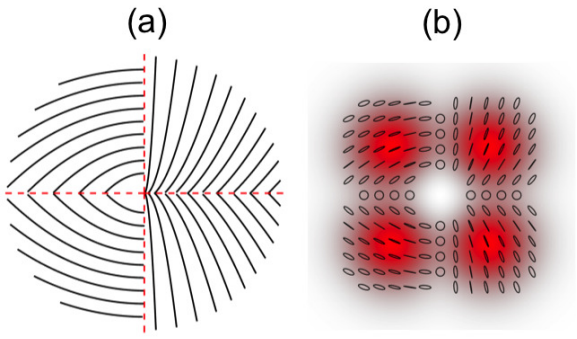

Figure 6. Example of a pattern containing C-lines. It correspond to the case $(2, -1)$ with $\beta = 45°$ and $\gamma = 180°$. Frame (a) shows the line pattern, whereas frame (b) shows the simulated mode with ellipses drawn throughout the mode. The dashed lines in (a) correspond to the C-lines.

Within each region bound by C-lines, the orientation of the semi major axes of the ellipse follows a curve, which is given in polar coordinates by

$$r = r_0 \left(\frac{C}{C_0} \right)^{-1/(\ell_2/2+1)}, \tag{22}$$

where r_0 is an initial value of r, C is given by

$$C = \cos[\phi(1 + \ell_2/2) + \pi/2 - \gamma/4 + \delta/2 - \phi_R/2], \tag{23}$$

and C_0 is C evaluated at the initial value $\phi = \phi_0$, with

$$\phi_R = \cos^{-1}\left(\text{sign}[\cos(\ell_1\phi - \gamma/2)]\right) \tag{24}$$

Figures 7 and 8 show the patterns for the case $\ell_1 = 2$ and $\ell_2 = -1$, for $\gamma = 0$ and $\gamma = 180°$, respectively. The patterns have radial lines drawn in solid red. The dashed red lines are the C-lines that appear in the $\beta = 45°$ pattern. The interesting aspect of this is that the patterns for $\beta \neq 0, 45°, 90°$ bear "scars" of C-lines. These scars are kinks in otherwise smooth patterns, at the directions of the C-lines. Scars underscore the fundamental construction of the mode via Eq. 1, which has its skeleton at $\beta = 45°$. Other patterns for $\beta \neq 45°$ bear signs of it because the line orientation changes nonlinearly due to the nonlinearity of the phase of the right-polarization:

$$\varphi_R = \tan^{-1}\left(\tan(\ell_1\phi - \gamma/2)\frac{1 - \tan\beta}{1 + \tan\beta}\right), \tag{25}$$

which has its greatest variation when $\phi = \phi_n$, as given by Eq. 21. As β increases or decreases further away from $\beta = 45°$, the intensity of the scars of C-lines decreases. When β reaches the values of the extreme symmetric patterns (0 and 90°), $\varphi_R = \pm(\ell_1\phi - \gamma/2)$, and the patterns show no scars. Moreover, if we just focus on the C-lines of the $\beta = 45°$ case we see that the C-lines are singular in ellipse orientation: the orientation of the line changes abruptly from one value to the other. Yet the lines do not need to be orthogonal, as is the case for $(1, 0)$.[5, 19]

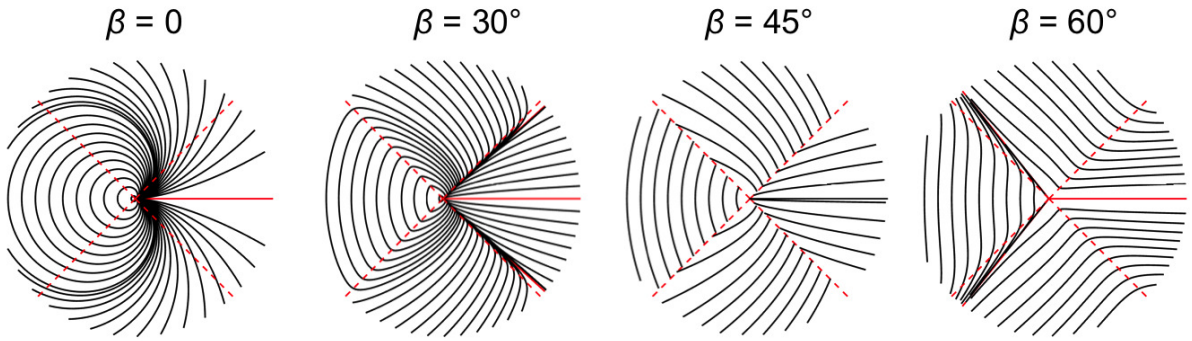

Figure 7. Scars seen in the case $\ell_1 = 2$ and $\ell = -1$ for $\gamma = 0$ and several values of β for each case. Red solid lines denote radial lines and red dashed lines denote the C-lines for the $\beta = 45^\circ$ case.

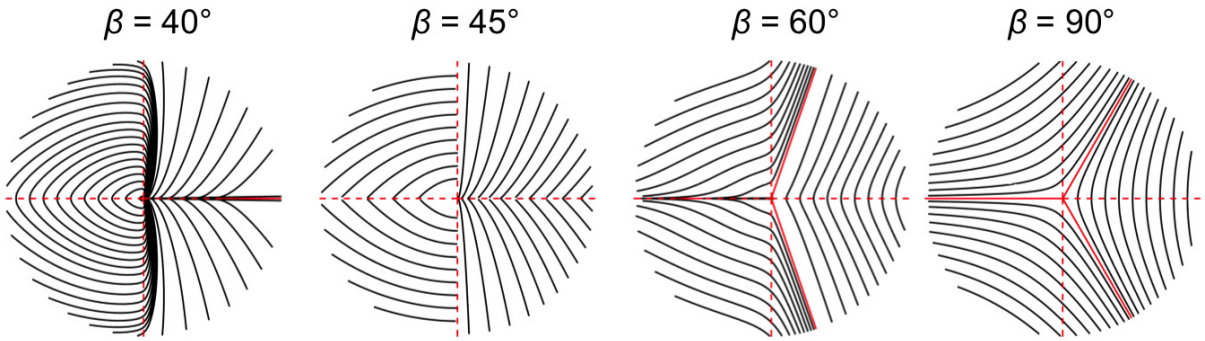

Figure 8. Scars seen in the case $\ell_1 = 2$ and $\ell = -1$ for $\gamma = 180^\circ$ and several values of β for each case. Red solid lines denote radial lines and red dashed lines denote the C-lines for the $\beta = 45^\circ$ case.

6. SUMMARY AND CONCLUSIONS

Up to now, monstars had been understood as a blend of lemons and stars: same sign of singularity index as lemons and same number of radial lines as star. The case involving $\ell_1 = 1$ and $\ell_2 = 0$, which was heavily studied before, had monstars as the intermediate case between lemons and stars.[5, 15, 20] Its name is indeed a blend of lemon and star. However, when we move to study hyper-C-points we can no longer say that the monstar has the same number of radial lines as the star, and a distinct number of radial lines as the lemon, because then we ask: which star or which lemon? Hyperlemons can have a large number of radial lines, as given by Eq. 11. The same is the case with hyperstars. Moreover, we have found a new regime where monstars are now a transitional pattern within lemons or stars. This marks a distinct realization: that there are monstars with a *negative* singularity index. This is a new regime that to our knowledge has not been realized before. Therefore, we must now see monstars more of a pattern of its own. Figure 3 shows a few cases of hypermonstars. That is, monstars with a high singularity index. If we focus on the shape of the line pattern we see only one distinctive feature: monstars have one or more sectors, bounded by radial lines, where the lines curve but radiate from center C-point, which has a positive or negative singularity. After the analysis of the case $I_C = 1$ we cannot even state that a monstar has to also have lemon-type sectors or star-like sectors, because that case does not have any; it is all monstar. Thus, the monstar ceases to be a blend of lemon or star. It is its own monst*e*r.

Finally, we note that the asymmetric patterns have intriguing shapes. More intriguing is that as they become more asymmetric they bear scars of a pattern of C-lines that is the midpoint in the transformation from one type of C-point to another. We have also done measurements for all of the cases presented here, but because of

limitations of space they will be presented elsewhere. To our knowledge these results are new and have not been reported before. At a fundamental level, they may lead to a better understanding of disclinations, which have parallels, for example, in liquid crystals.[21] In fact, disclinations in liquid crystals are in turn starting to be used purposefully as a way manipulate light.[22–24]

ACKNOWLEDGMENTS

This work was supported by National Science Foundation grant PHY -1506321.

REFERENCES

1. Maurer, C., Jesacher, A., Fürhapter, S., Bernet, S., and Ritsch-Marte, M., "Tailoring of arbitrary optical vector beams," *New J. Phys.* **9**, 78 (2007).
2. Wang, X.-L., Ding, J., Ni, W.-J., Guo, C.-S., and Wang, H., "Generation of arbitrary vector beams with a spatial light modulator and a common path interferometric arrangement," *Opt. Lett.* **32**, 3549–3551 (2007).
3. Galvez, E. J., Khadka, S., Schubert, W. H., and Nomoto, S., "Poincaré-beam patterns produced by non-separable superpositions of Laguerre-Gauss and polarization modes of light," *Appl. Opt.* **51**, 2925–2934 (2012).
4. Kumar, V., Philip, G. M., and Viswanathan, N. K., "Formation and morphological transformation of polarization singularities: hunting the monstar," *J. Opt.* **15**, 044027 (2013).
5. Galvez, E. J., Rojec, B. L., Kumar, V., and Viswanathan, N. K., "Generation of isolated asymmetric umbilics in light's polarization," *Phys. Rev. A* **89**, 031801 1–4 (2014).
6. Khajavi, B. and Galvez, E. J., "Preparation of Poincaré beams with a same-path polarization/spatial-mode interferometer," *Opt. Eng.* **54**, 111305 1–6 (2015).
7. Otte, E., Schlickriede, C., Alpmann, C., and Denz, C., "Complex light fields enter a new dimension: holographic modulation of polarization in addition to amplitude and phase," *Proc. SPIE* **9379**, 937908 (2015).
8. Cardano, F., Karimi, E., Slussarenko, S., Marrucci, L., de Lisio, C., and Santamato, E., "Polarization pattern of vector vortex beams generated by q-plates with different topological charges," *Appl. Opt.* **51**, C1–C6 (2012).
9. Cardano, F., Karimi, E., Marrucci, L., Lisio, C., and Santamato, E., "Generation and dynamics of optical beams with polarization singularities," *Opt. Express* **21**, 8815–8820 (2013).
10. Beckley, A. M., Brown, T. G., and Alonso, M. A., "Full Poincaré beams," *Opt. Express* **18**, 10777–10785 (2010).
11. Viswanathan, N. and Inavalli, V., "Generation of optical vector beams using a two-mode fiber," *Opt. Lett.* **34**, 1189–1191 (2009).
12. Jayarsuya, Y. V., Inavalli, V. V. G. K., and Viswanathan, N. K., "Polarization singularities in the two-mode optical fiber output," *Appl. Opt.* **50**, E131–E137 (2011).
13. Niv, A., Biener, G., Kleiner, V., and Hasman, E., "Rotating vectorial vortices produced by space-variant sub wavelength gratings," *Opt. Lett.* **30**, 2933–2935 (2005).
14. Nye, J., [*Natural Focusing and Fine Structure of Light*], Institute of Physics (1999).
15. Berry, M. and Hannay, J., "Umbilic points on Gaussian random surfaces," *J. Phys. A* **10**, 1809–1821 (1977).
16. Dennis, M., "Polarization singularities in paraxial vector fields: morphology and statistics," *Opt. Commun.* **213**, 201–221 (2002).
17. Freund, I., "Polarization singularity indices in Gaussian laser beams," *Opt. Commun.* **201**, 251–270 (2002).
18. Freund, I., "Polarization flowers," *Opt. Commun.* **199**, 47–63 (2001).
19. Galvez, E., Rojec, B., and Beach, K., "Mapping of all polarization-singularity C-point morphologies," *Proc. SPIE* **8999**, 89990I 1–8 (2014).
20. Dennis, M., "Polarization singularity anisotropy: determining monstardom," *Opt. Lett.* **33**, 2572–2574 (2008).
21. de Gennes, P. G. and Prost, J., [*The Physics of Liquid Crystals*], Clarendon Press (1993).
22. Stadler, M. and Schadt, M., "Linearly polarized light with axial symmetry generated by liquid-crystal polarization converters," *Opt. Lett.* **21**, 1948–1950 (1996).

23. Marrucci, L., Manzo, C., and Paparo, D., "Optical spin-to-orbital angular momentum conversion in inhomogeneous anisotropic media," *Phys. Rev. Lett.* **96**, 163905 1–4 (2006).
24. Brasselet, E., "Tunable optical vortex arrays from a single nematic topological defect," *Phys. Rev. Lett.* **108**, 087801 (2012).